



# Cyclic Behavior of Kaolin Clay under Undrained Conditions: Role of Microfabric

Quanyang Dong, Ph.D., Aff.M.ASCE<sup>1</sup>; Qi Sun, Ph.D., Aff.M.ASCE<sup>2</sup>; and Jun Yang, Ph.D., F.ASCE<sup>3</sup>

**Abstract:** The role of microfabric in the undrained cyclic behavior of kaolin clay is a topic of considerable interest but is yet to be fully understood. This paper presents new experimental data and analysis to address the topic. An efficient method is suggested to prepare flocculated and dispersed samples of good uniformity and repeatability in the laboratory. The experiments consistently show that there exists a critical cyclic stress ratio (CSR)—when the applied CSR is less than or greater than it, the accumulation of plastic strain and of residual pore water pressure during cyclic loading can be markedly different. The microfabric of kaolin clay affects the critical CSR, and this effect appears to be coupled with the effective confining pressure. In general, the flocculated sample has a larger critical CSR than the dispersed one and it has stronger resistance when subjected to CSR that is greater than the critical CSR. When subjected to CSR that is less than the critical CSR, the dispersed sample, however, exhibits larger resistance than the flocculated sample. Furthermore, the possible microscopic mechanism for the macroscopic experimental findings is explored by means of quantitative analysis of microfabrics of the flocculated and dispersed samples at different loading stages. **DOI: 10.1061/JGGEFK.GTENG-12838.** © 2025 American Society of Civil Engineers.

Author keywords: Clay; Cyclic loading; Microfabric; Plastic strain accumulation; Anisotropy.

#### Introduction

The structure of clay, including microfabric and bonding between soil particles, has an important influence on its overall mechanical behavior. The term microfabric refers to the arrangement of particle groups and pore spaces (Mitchell 1993). For natural clay, microfabric reflects the imprints of the geologic and stress history, the depositional environment, and the weathering history. Attempts have been made to find the differences in engineering properties between natural and remolded clays (Broms and Casbarian 1965; Kirkgard and Lade 1993). However, due to the complex environment of natural clay and the intricate effects of physical and chemical conditions on clay structure, it is difficult to identify the effect of microfabric in such comparative studies. To overcome the difficulty, attempts have been made to use different remolding methods in the laboratory, for example, using different consolidation pressures (Martin 1965) to obtain different microfabrics. Since the stress history has a significant influence on the mechanical properties of clay, it is also difficult to isolate the effect of microfabric. An alternative way is to use different pore water chemistry to form different microfabrics (Krizek et al. 1975; Soga 1994; Hazen and Penumadu 1999; Wang and Siu 2006). In general, clays

Note. This manuscript was submitted on March 23, 2024; approved on January 28, 2025; published online on May 14, 2025. Discussion period open until October 14, 2025; separate discussions must be submitted for individual papers. This paper is part of the *Journal of Geotechnical and Geoenvironmental Engineering*, © ASCE, ISSN 1090-0241.

deposited in salt water can develop a flocculated structure, whereas those deposited in fresh water have a dispersed structure (Lambe and Whitman 1969; Sachan and Penumadu 2007; Pillai et al. 2011).

Most of the existing experimental studies have concentrated on the effect of microfabric on the consolidation behavior of clay (Seed and Chan 1959; Sloane 1966; Mckyes 1971; Delage and Lefebvre 1984; Yu et al. 2016; Chow et al. 2019). A few studies also investigated the effect of microfabric on the shear behavior of clay (Wang and Siu 2006; Sachan and Penumadu 2007) and observed that flocculated clay samples had higher compressibility and lower shear strength compared with the dispersed samples. As far as the critical state line (CSL) is concerned, several studies showed that the CSL in the q-p' plane is independent of the initial microfabric of the sample (Wheeler and Sivakumar 2000; Pillai et al. 2011). Based on a qualitative comparison, Pillai et al. (2011) suggested that the microfabrics of flocculated and dispersed samples at critical state are similar. Several studies, however, showed that the microfabric can affect the CSL in the e-p' plane (Wheeler and Sivakumar 2000; Wang and Siu 2006). These diverse results indicate the complexity of the problem and call for further investigation.

In many practical applications, clay deposits are subjected to cyclic loading (e.g., wave loading, traffic loading, or seismic loading); it is thus important to properly determine the mechanical properties of clays under cyclic loading (Seed and Chan 1966; Sangrey et al. 1978; Idriss et al. 1980; Yasuhara and Andersen 1991; Hyde et al. 1993; Guo et al. 2013). By means of resonant column testing, several studies reported that soil structure can affect the shear modulus and damping ratio of clay (Edil and Luh 1980; Du et al. 1986; Wang and Siu 2006). However, the effect of microfabric on the cyclic behavior of clay has received much less attention (Pillai et al. 2011) and is not yet fully understood. Most of the prior studies on the effect of soil fabric have focused mainly on the cyclic behavior and liquefaction resistance of sands (e.g., Sze and Yang 2014). For clays, changes of the depositional environment may alter their microfabric, and hence it is of interest to explore the cyclic behavior and strength of clay with different microfabric.

<sup>&</sup>lt;sup>1</sup>Research Associate, Dept. of Civil Engineering, The Univ. of Hong Kong, Hong Kong, China; currently, Associate Professor, College of Civil Engineering and Architecture, Wenzhou Univ., Wenzhou 325035, China. ORCID: https://orcid.org/0000-0002-9104-1347

<sup>&</sup>lt;sup>2</sup>Research Associate, Dept. of Civil Engineering, The Univ. of Hong Kong, Hong Kong, China; currently, Associate Professor, College of Civil Engineering and Architecture, Wenzhou Univ., Wenzhou 325035, China.

<sup>&</sup>lt;sup>3</sup>Professor, Dept. of Civil Engineering, The Univ. of Hong Kong, Hong Kong, China (corresponding author). ORCID: https://orcid.org/0000-0002-0250-5809. Email: junyang@hku.hk

This paper presents new experimental data aimed to better understand the effect of microfabric on the behavior of kaolin clay under undrained cyclic loading. An efficient method was developed to prepare quality kaolin clay samples with flocculated and dispersed microfabrics in the laboratory. A series of stress-controlled cyclic triaxial tests was carried out on flocculated and dispersed samples, and the results in terms of pore pressure response and plastic strain accumulation were analyzed in detail. Furthermore, the microfabrics of flocculated and dispersed samples were quantified using an imaging technique to explore the microscopic mechanisms for the observed behavior.

# **Preparing Remolded Clay Samples**

#### **Principles**

Commercially available kaolinite obtained from Suzhou, China, was used in the present study. The kaolin clay has a specific gravity of 2.61, with 80% of particles being finer than 10  $\mu m$  and 46% finer than 2  $\mu m$ , with activity of 0.44. The reason for choosing commercial kaolin clay instead of natural clay is to minimize the uncertainty associated with different minerals in natural clay. Kaolinite is a kind of stable clay mineral that does not swell or expand when encountering water.

Kaolinite is a 1:1 sheet silicate, composed of a  $(\mathrm{Si_2O_5})^{-2}$  tetrahedral layer and an  $(\mathrm{Al_2[OH]_4})^{+2}$  octahedral layer. When kaolin clay is in acidic aqueous solution, the faces of the particles get negatively charged while the edges get positively charged. In this case, the edges of a platelet can be attracted to the faces of another platelet, and meanwhile the faces of the platelets try to repel each other as far as possible. As a result, these platelets form a flocculated microfabric (Carty 1999). However, dispersant solution can change the charges carried at the edges of the particle. The anions ionized by the dispersant have priority to be adsorbed at the edges (Carty 1999), thus making the side negatively charged. All of the particles carry negative charges, leading to repulsion between each other. Therefore, the parallel particles caused by repulsion result in a dispersed microfabric when subjected to consolidation pressure.

# Sample Preparation

In preparing the kaolin slurry, the water content was about two times the liquid limit of the clay. The kaolin powder was mixed with distilled water for the flocculated microfabric, whereas it was mixed with dispersant solution prepared by dissolving 2% Calgon by weight for the dispersed microfabric.

In most experimental studies, the method of one-dimensional slurry consolidation was employed to prepare clay samples with different microfabrics (Sachan and Penumadu 2007; Pillai et al. 2011; Wang and Siu 2006). This conventional method has several limitations. First, the slurry may easily leak from the consolidometer when high stresses are applied, especially for the slurry with dispersant. Second, it usually takes a long time to complete consolidation for samples with dispersed microfabric. In addition, nonuniformity can become significant when the method is used to prepare large samples.

To overcome these disadvantages, a tailor-made vacuum consolidation device was set up in this study, as schematically shown in Fig. 1. The device is composed of a cylindrical mould with pedestal and porous plate at the bottom, a graduated cylinder, and a vacuum pump. The graduated cylinder is to measure the amount of water consolidated from the slurry. The digital vacuum pump

provides specific consolidation pressures. Each sample is placed in an individual mould, and several samples as a batch (e.g., eight samples in this study) can be prepared simultaneously by joining all the pedestals as a circuit. Note that in this study filter papers were placed on the top, bottom, and around the slurry to speed up consolidation.

After pouring the slurry into the rubber membrane inside the cylindrical mould, the top of the rubber membrane was fastened by rubber band to form a sealed state in order to prevent leakage during consolidation. The preparation of kaolin samples with the different microfabrics adopted the same consolidation pressure. The slurry was initially consolidated under the vacuum pressure of 15 kPa; after the finish of consolidation, it was continued to consolidate by increasing the vacuum pressure by 15 kPa in steps until the completion of consolidation under 90 kPa.

By using the specifically designed device, a batch of samples can be prepared simultaneously to ensure uniformity and repeatability. Each specimen after consolidation was measured 80 mm in diameter and 150 mm in height. The vacuum consolidation method can significantly shorten the time as compared with the conventional method. In general, it took five days to prepare floculated samples and eight days to prepare dispersed samples.

Table 1 summarizes the physical properties of the flocculated and dispersed samples. Note that the flocculated sample has lower density, higher water content, and higher permeability than the dispersed sample. The liquid limit of the flocculated sample is higher than that of the dispersed sample, but the plastic limit is almost the same. These results are consistent with those reported by Sachan and Penumadu (2007) and Pillai et al. (2011).

To examine the microfabric of the prepared samples, SEM images of the samples after consolidation under vacuum pressure of 90 kPa were taken along the vertical direction (i.e., the direction of major principal stress in triaxial compression test), as shown in Fig. 2. These images confirm that the flocculated sample has a random orientation of clay platelets with face-to-edge contact [Fig. 2(a)], whereas the dispersed microfabric is in the form of layered arrangement of clay platelets with face-to-face contact [Fig. 2(b)]. The observations are in agreement with those reported in previous studies (Sides and Barden 1971; Sachan and Penumadu 2007; Pillai et al. 2011). Further quantification of the microfabric

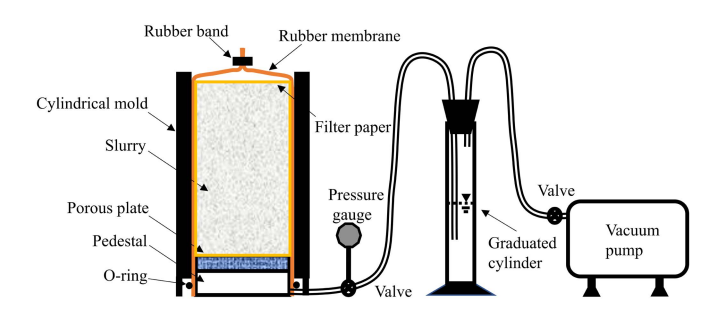


Fig. 1. Schematic of the vacuum consolidation device for the study.

Table 1. Physical properties of flocculated and dispersed samples

	Initial	Water		Initial void	Liquid	Plastic
Sample	density,		Permeability, <i>k</i> (cm/s)			limit, $w_P$ (%)
Sample	$\rho_0$ (g/cm <sup>2</sup> )	W (%)		$e_0$	$W_L$ (%)	W <sub>P</sub> (%)
Flocculated	1.13	44.9	$1.4 \times 10^{-7}$	1.30	60.8	24.1
Dispersed	1.25	38.2	$3.8 \times 10^{-8}$	1.05	40.0	24.5

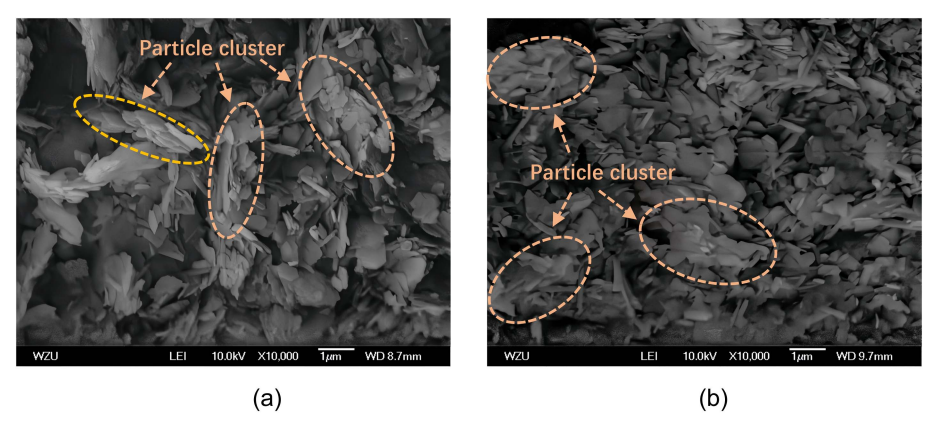


Fig. 2. SEM images of the kaolin clay used: (a) flocculated microfabric; and (b) dispersed microfabric.

will be presented later. It is worth noting that most of the flocculated structures look like the book-house instead of card-house structure. A more realistic representation of the dispersed structure is the turbostratic arrangement (Sides and Barden 1971).

One critical issue in the study of the effect of microfabric is to ensure uniformity and repeatability of the samples submitted to testing. To validate the quality of the prepared samples, the water content was measured for different parts. As shown in Fig. 3, a total of nine locations were selected for a test sample—three at the top, three in the middle, and three at the bottom. Typical test results are summarized in Table 2. For the flocculated sample, the water content varies between 44.3% and 45.9%, with an average value of 44.9%, while it ranges between 37.6% and 39.1% for the dispersed sample, with an average value of 38.2%. Both flocculated and dispersed samples showed excellent uniformity.

Furthermore, parallel triaxial compression tests were conducted on flocculated and dispersed samples under the effective confining pressure of 100 kPa. In doing so, cylindrical specimens 100 mm in height and 50 mm in diameter were extracted from the core of the

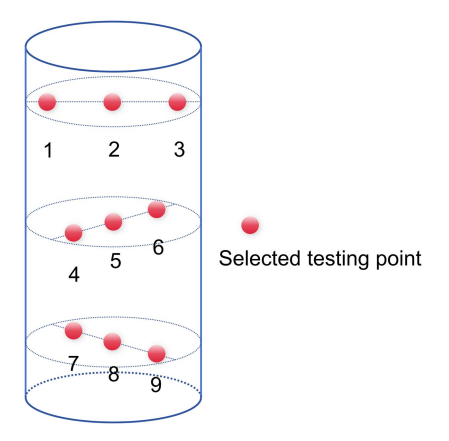


Fig. 3. Distribution of the selected points for water content measurement.

slurry-consolidated sediment. The test results are shown in Fig. 4(a), where F and D stand for the flocculated and dispersed samples, respectively. It is evident that the stress-strain relationships of the two parallel samples is quite consistent, confirming excellent repeatability and reliability of the experiments.

Fig. 4(b) shows the void ratio versus isotropic consolidation pressure for dispersed and flocculated samples. It is evident that the compressibility of flocculated and dispersed microfabric is significantly different. The compression index,  $C_{\rm C}$ , for the flocculated sample is much higher than the dispersed sample, but the swelling index,  $C_{\rm S}$ , is similar.

# **Testing Apparatus and Procedure**

The apparatus used in the present study is an advanced dynamic triaxial testing system that can realize static and dynamic tests under arbitrary stress paths. The cyclic load can be applied up to 5 Hz, and the deformation and pore pressure are measured via a robust real-time data acquisition system. Each specimen was saturated by circulation of deaired water and then by application of back pressure, and full saturation was assumed at the Skempton pore pressure parameter being greater than 0.96. The saturated specimen was isotropically consolidated to the specified confining pressure and then subjected to stress-controlled cyclic triaxial testing under undrained conditions. The frequency of cyclic loading was set as 0.1 Hz.

All samples were subjected to 5,000 cycles, except those that reached the axial strain level of 12% before 5,000 cycles. Cyclic triaxial tests were carried out under two effective confining pressures, 100 and 200 kPa. The applied cyclic stress ratio (CSR), defined as follows, was between 0.35 and 0.77:

$$CSR = \frac{q_d}{q_f} \tag{1}$$

where  $q_d$  = cyclic deviatoric stress; and  $q_f$  = undrained shear strength of the sample obtained from the monotonic loading test.

Table 2. Test results of water content (in %) of flocculated and dispersed samples

Sample	Point 1	Point 2	Point 3	Point 4	Point 5	Point 6	Point 7	Point 8	Point 9	Average water content
Flocculated	44.3	44.6	44.4	44.7	45	44.8	45.6	45.9	45.5	44.9
Dispersed	37.6	37.8	37.7	38.0	38.3	38.1	39	39.1	38.8	38.2

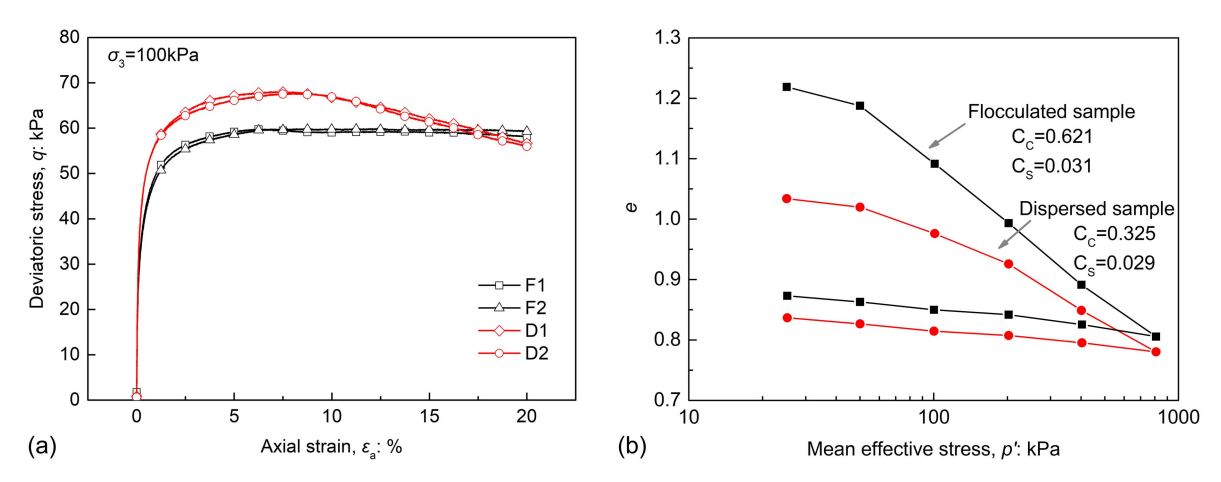


Fig. 4. Test results on flocculated and dispersed samples: (a) stress-strain curves in triaxial loading; and (b) variation of void ratio under isotropic consolidation.

# **Test Results**

# Monotonic Loading Tests

Monotonic tests were conducted at the strain rate of 0.05 mm/min under effective confining pressure of 100 and 200 kPa, respectively. Fig. 5(a) shows the stress–strain curves of flocculated and dispersed samples under two different confining pressures, and Fig. 5(b) shows the pore pressure responses of these specimens. It is interesting to note that the dispersed samples exhibit strain softening behavior, whereas the flocculated samples show strain hardening response. The maximum deviatoric stresses of the dispersed samples at the confining pressure of 100 and 200 kPa are determined as 68.1 and 124.4 kPa, respectively. By comparison, the maximum deviatoric stresses of the two flocculated samples are 59.4 and 119.9 kPa. As far as the excess pore pressure is concerned, higher pore pressures were generated in the flocculated samples, implying that the flocculated samples were more contractive than the dispersed samples.

The effective stress paths of the flocculated and dispersed sample for the monotonic test under 100, 150, and 200 kPa are shown in Fig. 6(a), and the CSL and normal consolidation line (NCL) of the flocculated and dispersed samples are plotted in the  $q-p^\prime$  and  $v-p^\prime$  space. As shown in Fig. 6, at a given confining pressure, two samples with different microfabrics arrive at different critical states.

The flocculated samples attain a larger critical stress ratio (q/p') in the q-p' plane and a steeper CSL in the v-p' space. The friction angles at the critical state determined are comparable with that reported by Prashant and Penumadu (2005). Moreover, the NCL is parallel to its own CSL, which is consistent with the test result on remolded clay by Wood (1990). The microfabric affects not only the consolidation response but also the behavior at the critical state.

# Cyclic Loading Tests

Table 3 summarizes the results of cyclic tests conducted on flocculated and dispersed samples, including final accumulated strains and residual pore pressures. As an example, Fig. 7 shows the results of a flocculated sample under the confining pressure of 100 kPa and the CSR of 0.57, where the plot of Fig. 7(a) presents the evolution of axial strain ( $\varepsilon_a$ ) with the number of cycles and the plot in Fig. 7(b) shows the buildup of excess pore pressure (u).

# **Plastic Strain Accumulation**

By subtracting the resilient strain  $(\varepsilon_p)$  from the total strain  $(\varepsilon_a)$ , the plastic strain  $(\varepsilon_p)$  can be derived. Fig. 8(a) shows the accumulated plastic strain  $(\varepsilon_p)$  as a function of number of cycles for flocculated and dispersed samples under the confining pressure of 100 kPa and subjected to CSR  $\leq$  0.57. Fig. 8(b) shows the accumulated plastic strain  $(\varepsilon_p)$  as a function of loading cycles at CSR greater than 0.57.

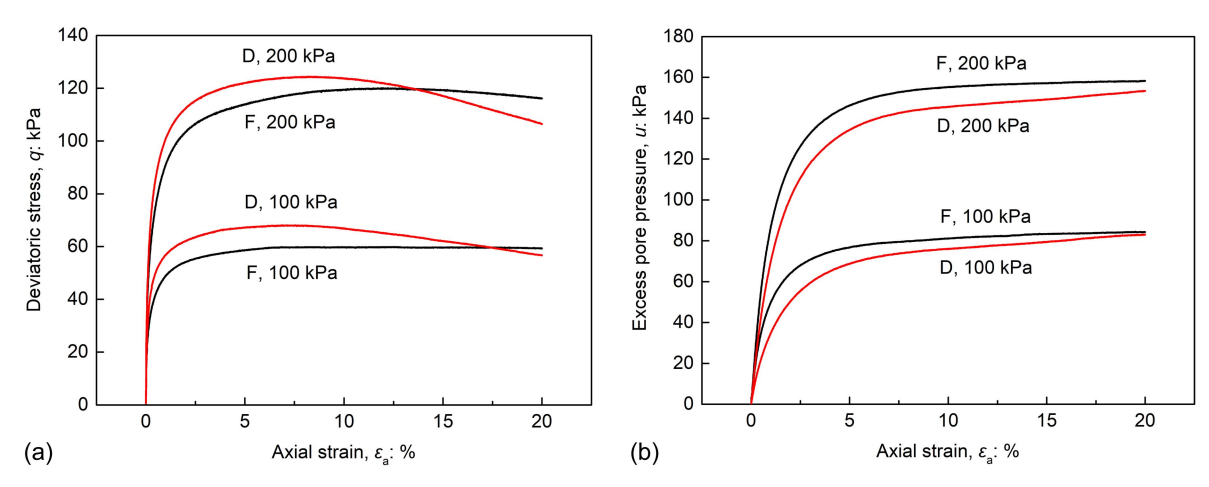
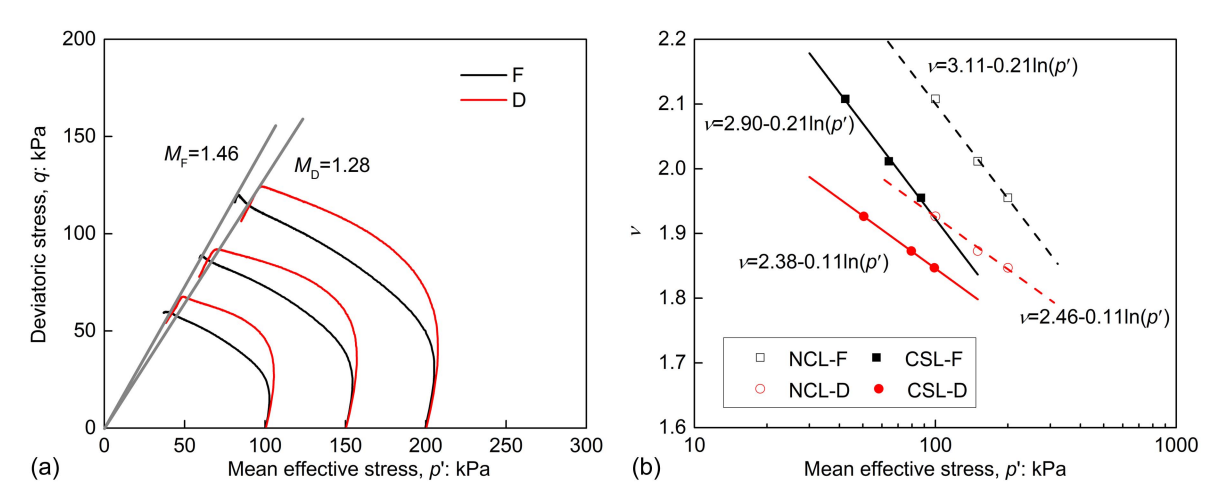


Fig. 5. Results of undrained triaxial compression tests: (a) stress-strain curve; and (b) pore pressure response.



**Fig. 6.** Test results of (a) effective stress path; and (b) CSL and NCL in v - p' space.

The corresponding results for the case of confining pressure of 200 kPa are shown in Figs. 9(a and b).

One of the notable findings is the effect of CSR. Take the case of confining pressure of 100 kPa (Fig. 8) as an example. When CSR  $\leq 0.57$ , plastic strain accumulates mainly at the first few hundred cycles, for both flocculated and dispersed samples, and then tends to remain at a stable strain level afterwards. The final plastic strains after 5,000 cycles are relatively small (less than 1.2%). In terms of the role of microfabric, flocculated samples undergo larger plastic strains than dispersed samples under the same CSR. For example, at CSR = 0.57, the cumulative plastic strain after 5,000 cycles is 1.15% for the flocculated sample as compared with 0.80% for the dispersed sample.

Table 3. Summary of cyclic triaxial tests

	Effective			
	confining			Final residual
	pressure,		Final accumulative	pore pressure,
Sample	$\sigma_3'$ (kPa)	CSR	strain, $\varepsilon_p$ (%)	$u_r$ (kPa)
Flocculated	100	0.35	0.216	23.01
Flocculated	100	0.50	0.517	45.67
Flocculated	100	0.57	1.147	57.84
Flocculated	100	0.63	2.718	86.89
Flocculated	100	0.70	12.000	98.93
Flocculated	100	0.77	12.000	97.44
Flocculated	200	0.35	0.350	43.80
Flocculated	200	0.50	1.041	72.87
Flocculated	200	0.57	1.878	134.77
Flocculated	200	0.63	6.173	179.59
Flocculated	200	0.70	12.000	184.45
Flocculated	200	0.77	12.000	178.46
Dispersed	100	0.35	0.144	21.97
Dispersed	100	0.50	0.430	41.53
Dispersed	100	0.57	0.801	54.38
Dispersed	100	0.63	12.000	83.57
Dispersed	100	0.70	12.000	49.02
Dispersed	100	0.77	12.000	49.85
Dispersed	200	0.35	0.186	39.92
Dispersed	200	0.50	0.528	67.25
Dispersed	200	0.57	12.000	173.85
Dispersed	200	0.63	12.000	171.01
Dispersed	200	0.70	12.000	100.75
Dispersed	200	0.77	12.000	83.42

However, when CSR is greater than 0.57, a markedly different phenomenon is observed, as shown in Fig. 8(b). In the case of CSR = 0.63, for example, the dispersed sample develops plastic strain relatively more slowly than the flocculated sample at the first few hundred cycles, but as the cyclic loading further proceeds, a rapid development of plastic strain takes place in the dispersed sample and the deformation becomes uncontrollable at the 645th cycle. By comparison, the plastic strain continues to accumulate gradually in the flocculated sample, reaching ~2.72% at the end of 5,000 cycles, and it does not appear to reach a stable strain level. When CSR is increased to 0.70, the dispersed sample becomes uncontrollable more rapidly, at the 38th cycle, whilst the flocculated sample also develops large plastic strains (~12%) well before the specific number of cycles (5,000) is reached.

Similar observations can be obtained in the case of effective confining pressure of 200 kPa (Fig. 9). An additional point of interest is that the dispersed sample under the CSR of 0.57 develops uncontrollable deformation at the 3048th cycle, whereas under the same CSR but at the confining pressure of 100 kPa, it shows a kind of stable response, with the accumulated plastic strain of less than 1.2% after 5,000 cycles of loading. This finding reveals the interplay of the CSR and the effective confining pressure.

#### **Residual Pore Pressure**

Figs. 10 and 11 present the residual pore pressure  $(u_r)$  as a function of number of cycles for flocculated and dispersed samples under the confining pressure of 100 and 200 kPa, respectively. The values of residual pore pressures at the end of the tests are given in Table 3.

Under the confining pressure of 100 kPa and at the CSR of less than 0.57, the development of residual pore pressure in flocculated and dispersed samples shows a similar pattern [Fig. 10(a)]: the residual pore pressure builds up in the first few hundred cycles and then tends to stabilize afterwards. Overall, larger pore pressures are generated in flocculated samples than in dispersed samples under otherwise similar conditions, implying that flocculated samples are more contractive than dispersed samples. This result is consistent with the finding obtained from the undrained monotonic tests [Fig. 5(b)].

When the applied CSR is greater than 0.57, the accumulation of residual pore pressure shows significantly different patterns in flocculated and dispersed samples [Fig. 10(b)]. The residual pore pressure builds up rapidly toward failure in dispersed samples, whereas in flocculated samples it builds up quickly in the first several hundred cycles and then tends to stabilize afterwards. At the

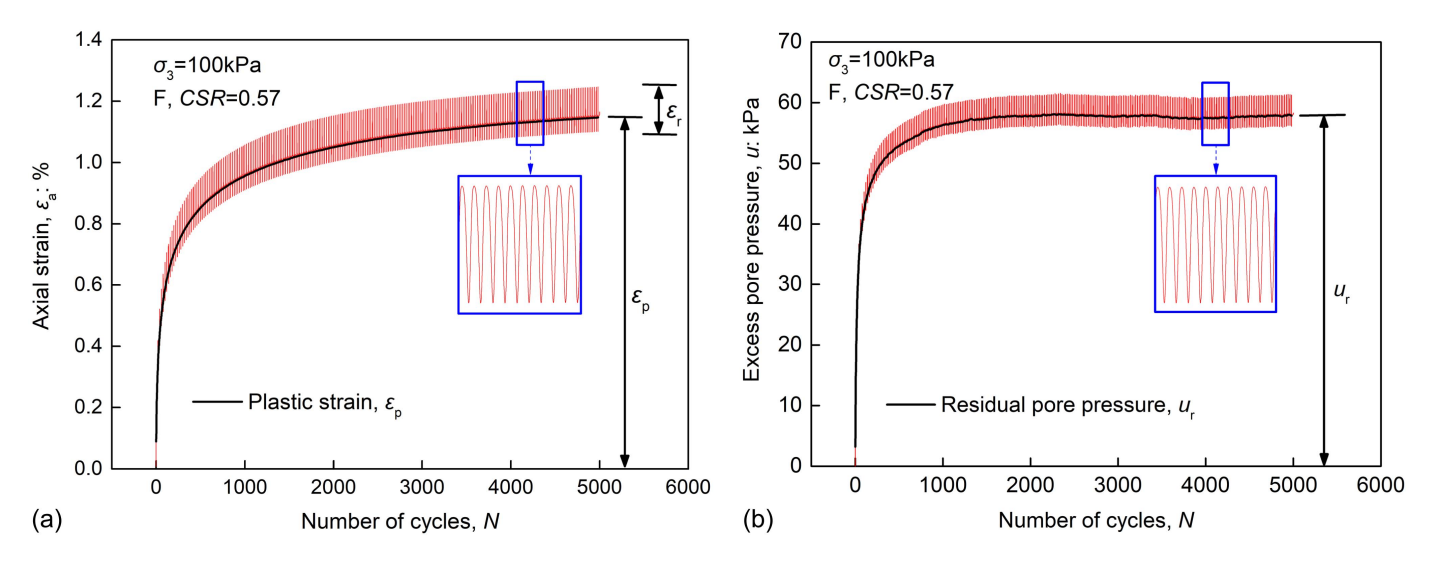
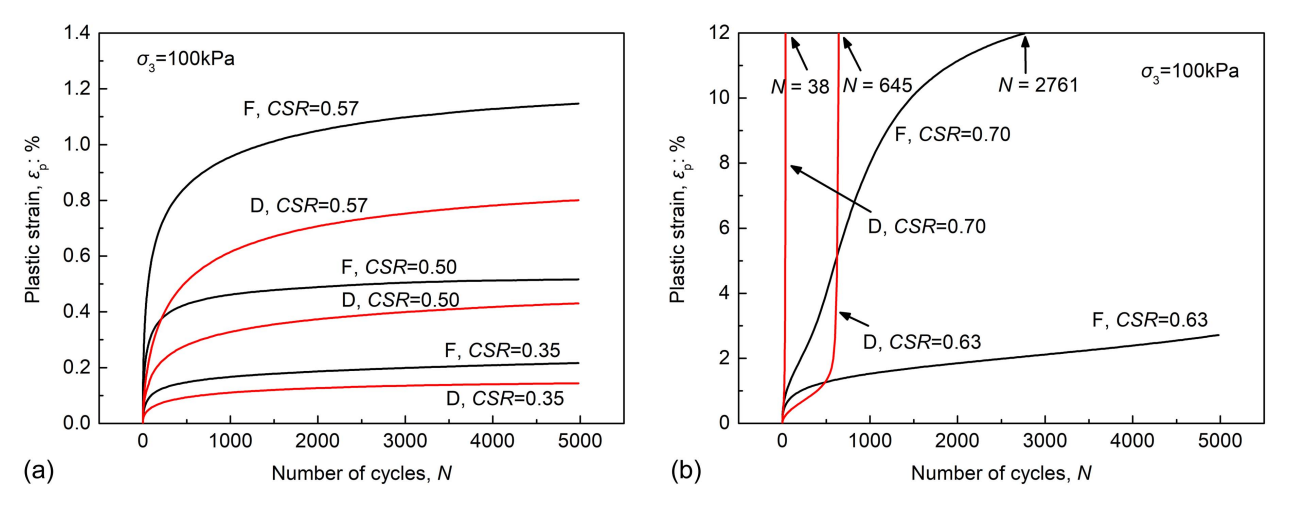


Fig. 7. Typical results of flocculated sample ( $\sigma_3 = 100$  kPa, CSR = 0.57): (a) development of axial strain; and (b) development of excess pore pressure.



**Fig. 8.** Accumulation of plastic strains of flocculated and dispersed samples under effective confining pressure of 100 kPa: (a) CSR = 0.35-0.57; and (b) CSR > 0.57.

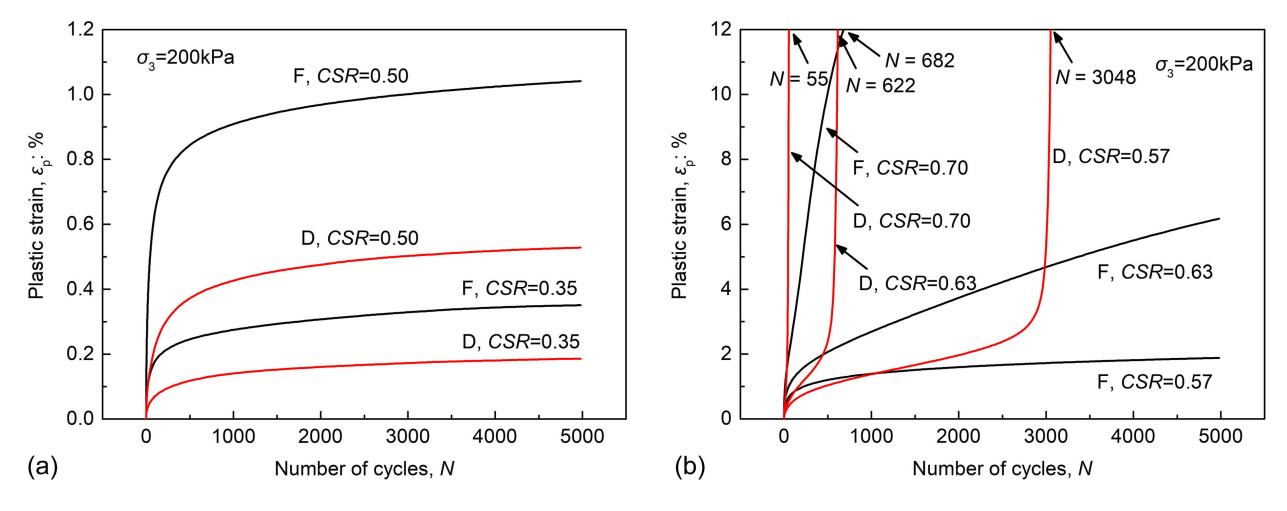
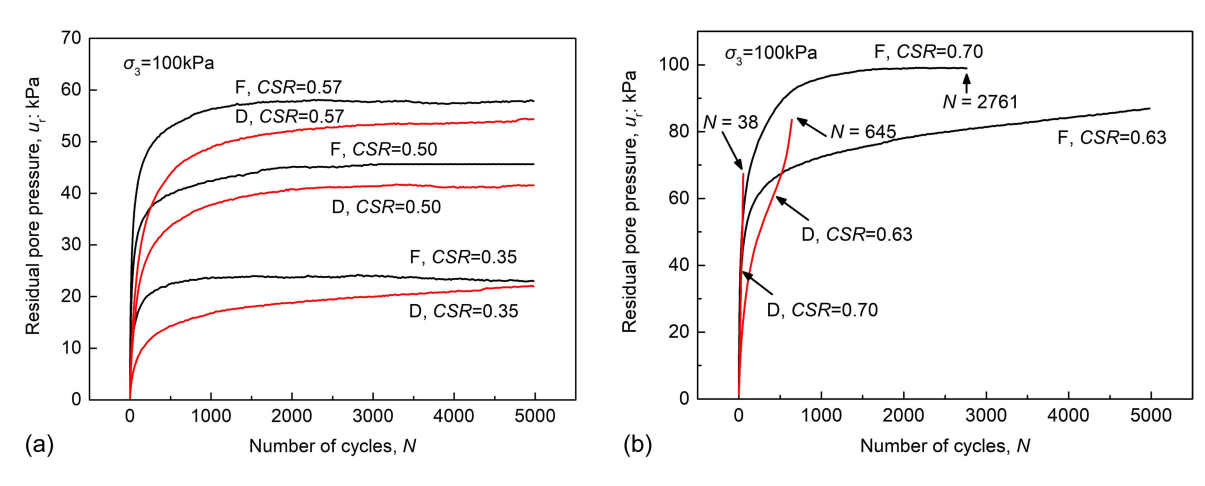


Fig. 9. Accumulation of plastic strains of flocculated and dispersed samples under effective confining pressure of 200 kPa: (a) CSR = 0.35-0.50; and (b) CSR > 0.50.



**Fig. 10.** Development of residual pore pressure of flocculated and dispersed samples under effective confining pressure of 100 kPa: (a) CSR = 0.35-0.57; and (b) CSR > 0.57.

CSR of 0.70, for example, the residual pore pressure in the flocculated sample becomes close to the effective confining pressure at around 1,000 cycles and then remains almost unchanged until the end of the test. By comparison, the dispersed sample fails at the 38th cycle with the recorded residual pore pressure of ~70 kPa.

Similar observations can be obtained in the case of effective confining pressure of 200 kPa (Fig. 11). It is worth noting that the dispersed sample under CSR = 0.57 shows a markedly different feature as compared with the dispersed sample under the *same* CSR but *lower* confining pressure, indicating the interplay of the effects of CSR and the confining pressure.

#### Critical Cyclic Stress Ratio and Cyclic Strength

The results in Figs. 8–11 suggest that there exists a critical CSR, which can be regarded as the maximum CSR that does not lead to failure (Larew and Leonards 1962; Sangrey et al. 1978). If assuming the failure criterion of 5% plastic strain, the values of critical CSR of the flocculated and dispersed samples under the effective confining pressure of 100 kPa can be determined as 0.63 and 0.57, respectively, and the critical CSR values under the confining pressure of 200 kPa are 0.57 and 0.50, respectively. Note that these critical values are approximate estimates based on the test results. Therefore, it can be concluded that the microfabric of kaolin clay affects the critical CSR, and this effect is coupled with the effective

confining pressure. In general, the flocculated sample has a larger critical CSR than the dispersed one, meaning that it is more difficult to fail the flocculated sample, especially under low effective confining pressure.

As defining cyclic strength for sand (Yang and Sze 2011), similar cyclic strength curves can be determined for the kaolin clay, as shown in Fig. 12, where  $N_f$  is defined as number of loading cycles to failure (5% accumulated plastic strain). One can notice that the cyclic strength of floculated samples is larger than that of dispersed samples. Furthermore, the cyclic strength difference due to different microfabrics slightly decreases with increasing confining pressure. This may be due to rearrangement of aggregates associated with confining pressures (Sachan and Penumadu 2007).

## **Plastic Strain Development Patterns**

Based on a thorough examination of the tests conducted, three types of deformation patterns can be put forward for flocculated and dispersed samples, respectively, as shown in Fig. 13.

Fig. 13(a) shows the three patterns of flocculated samples. When CSR is smaller than the critical CSR, the plastic strain accumulates toward a stable level after a few hundred loading cycles (Type I). When CSR is close to the critical CSR, the plastic strain accumulates gradually until the end of the test (Type II). When CSR is larger than the critical CSR, plastic strain accumulates more

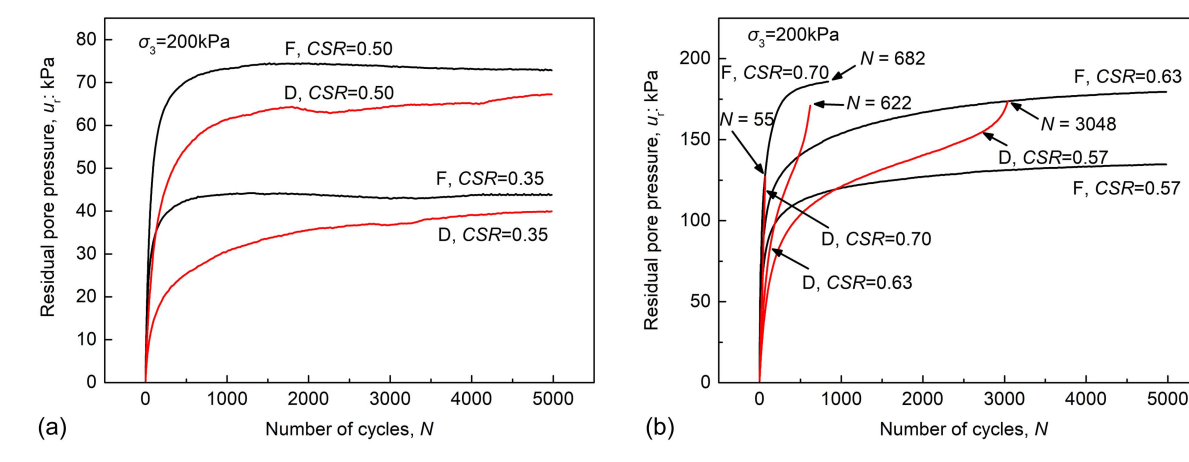


**Fig. 11.** Development of residual pore pressure of flocculated and dispersed samples under effective confining pressure of 200 kPa: (a) CSR = 0.35-0.50; and (b) CSR > 0.50.

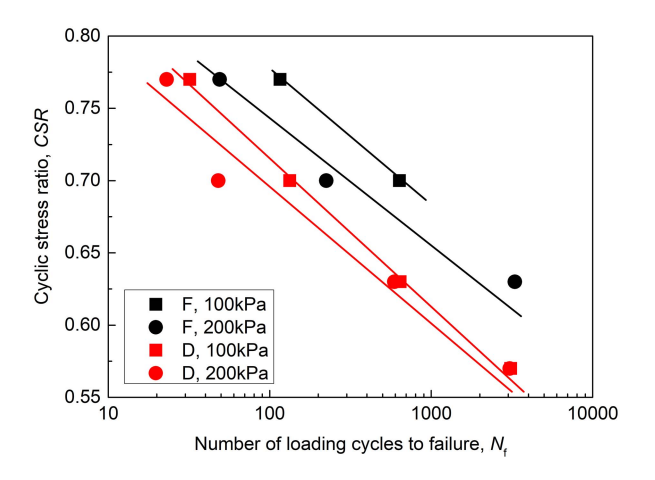


Fig. 12. Cyclic strength curves of flocculated and dispersed samples.

quickly in the initial stage of loading and then accumulates at a decreased rate (Type III).

The three patterns of dispersed samples are shown in Fig. 13(b). When CSR is smaller than critical CSR, the pattern is similar to Type I of flocculated samples. When CSR is close to the critical CSR, the plastic strain accumulation is relatively slow in the initial stage, which is followed by a rapid development of large strain leading to failure (Type II'). When CSR is larger than the critical CSR, a rapid development of plastic strain toward failure may occur within the first few cycles (Type III').

The markedly different patterns between Type II and Type II' and between Type III and Type III' highlight the significant effect of microfabric on the undrained cyclic behavior of kaolin clay.

#### **Quantification of Microfabric**

To further understand the observed differences in the behavior of flocculated and dispersed samples, an attempt was made to quantify their microfabrics using SEM image processing. It is to be acknowledged that the 2D nature of SEM images poses an intrinsic limitation. While 3D characterization techniques, such as microscopic-computed tomography scanning, are now available, it remains a challenge to acquire microstructural information accurately. To overcome the limitation of the 2D SEM images, both horizontal and vertical SEM images are analyzed and processed in this study.

# Sample Preparation for Image Processing

To explore the linkage between the macroscopic behavior and the microfabric, three states were investigated for both flocculated and dispersed samples, that is, (a) initial state (after preparation in the consolidation device); (b) after isotropic consolidation (i.e., 200 kPa) in the triaxial apparatus; and (c) 15% axial strain after undrained monotonic tests. All the samples reached their critical states approximately at 15% axial strain, with a constant stress ratio and reasonable homogeneity. In order to take SEM images of the microstructure of each specimen, the specimen was withdrawn from the cell by slowly reducing the stress under undrained conditions such that any potential influence of unloading was minimized.

A schematic illustration of sample preparation for SEM analysis is given in Fig. 14. A rectangular soil slice ( $10 \text{ mm} \times 10 \text{ mm} \times 20 \text{ mm}$ ) was extracted from the core, and the samples were quickly frozen by liquid nitrogen, and then were placed in a freeze dryer at a temperature of  $\sim 50^{\circ}\text{C}$  to remove water by sublimation. And the samples for vertical and horizontal SEM observation were notched in the middle section perpendicular to the horizontal direction (y-direction) and vertical direction (z-direction). The freeze-drying method is considered most appropriate for dehydrating clayey soil samples, especially clays of kaolinite type, without disturbing fabric (Delage and Pellerin 1984).

SEM images were taken by a ZEISS scanning electron microscope (Sigma 300), which has a resolution of 1.0 nm and a maximum magnification of 1,000,000. A magnification factor of ×10,000 and an accelerating voltage of 2.0 kV were used to capture high-resolution SEM images. Ten SEM images were taken from each observational plane. In each SEM image, approximately more than 400 pores were identified, and at least 4,000 pores were analyzed in total for one single observational plane. This number of pores is considered sufficient to provide a good representation of fabric components (Chow et al. 2019; Tang et al. 2020).

The software, Pores (Particles) and Cracks Analysis System, was employed in this study. SEM images were first converted into binary images using the global thresholding method (Sokolov et al. 1998; Prakongkep et al. 2010), in which the voids and solids (particles and aggregates) were represented by white and black, respectively. Second, isolated pores were identified using the seed filling algorithm or the improved scan line seed filling algorithm. Erosion operation was applied to separate the connected pores (Liu et al. 2011). It should be noted that very small pores cannot be identified as measurements on small objects are incorrect due to a small number of pixels. Also, some small dots are impurities and image

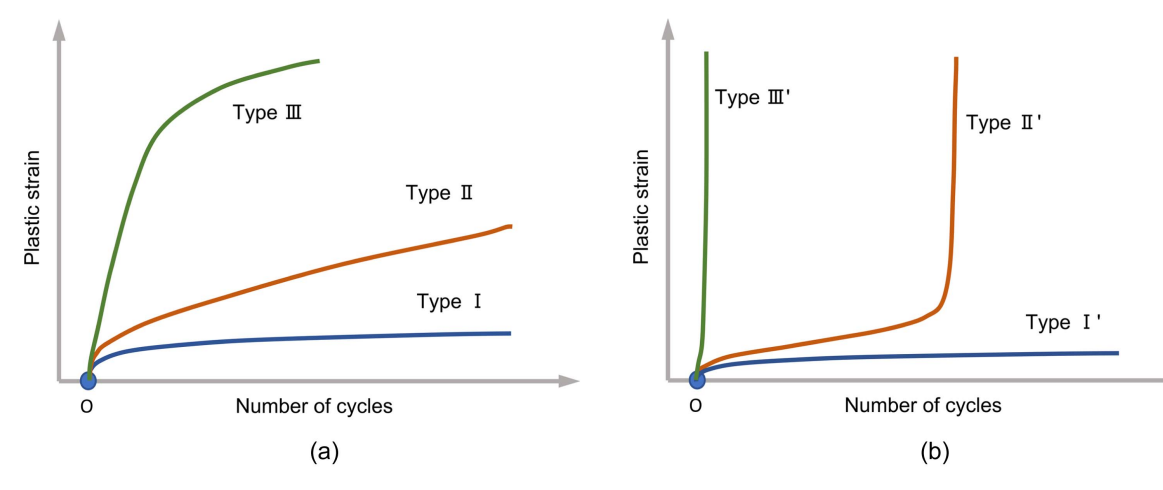


Fig. 13. Schematics of plastic strain development of (a) flocculated samples; and (b) dispersed samples.

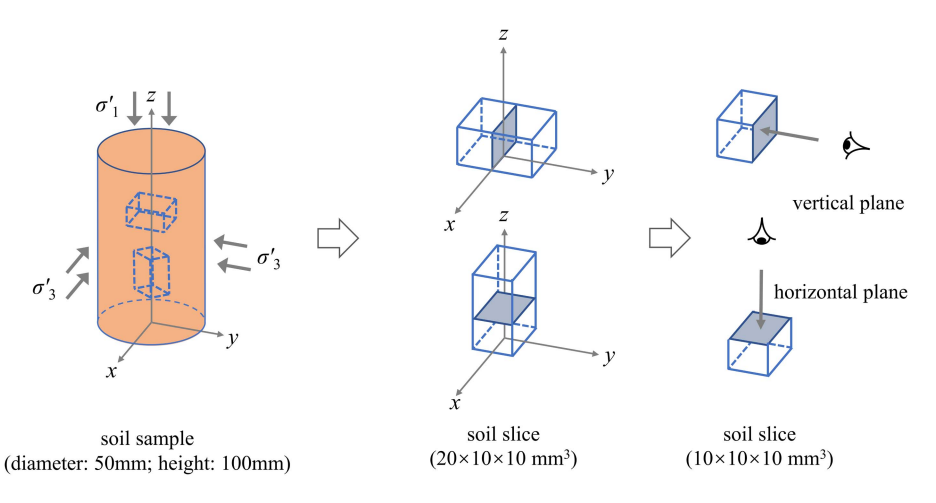


Fig. 14. Schematic of sample preparation for SEM observation.

Table 4. Statistical parameters of the micropores from SEM images at initial state

Sample	Total region area ( $\mu$ m <sup>2</sup> )	Total Region number	Porosity	Average region area (μm²)	Average perimeter (μm)	Average length (μm)	Average width (μm)
Flocculated-horizontal-vertical	221.960	5875	0.255	0.038	0.976	0.312	0.166
Flocculated	152.233	4999	0.175	0.030	0.863	0.298	0.149
Dispersed-horizontal	155.056	6667	0.178	0.023	0.787	0.268	0.139
Dispersed-vertical	176.727	6964	0.203	0.026	0.825	0.281	0.145

noise. Therefore, the pores represented by less than 50 pixels (0.006  $\mu$ m × 0.006  $\mu$ m) were removed. After SEM image processing, the pore geometric parameters (e.g., the pore area, the pore perimeter, the major and minor axis lengths, and the direction) were computed (Table 4). As an example, the original SEM image, binary image, and processed vector image are shown in Fig. 15.

#### Quantitative Analysis

It is of interest to analyze pore orientation and pore shape (i.e., pore roundness). Pore orientation is defined as the direction of the major axis of a pore with respect to the horizontal rightward direction, which is perpendicular to the axial stress applied in triaxial tests. In order to quantify the frequency of pore orientation at a given angle range  $(\theta_i)$ , the angle  $(\theta)$  from  $0^\circ$  to  $360^\circ$  is divided into 24 equal intervals. Therefore, the percentage of pores with  $\theta_i$  orientation is calculated by

$$p(\theta_i) = \frac{N_{\theta_i}}{N} \times 100\% \quad (i = 1, 2, 3, \dots, 24)$$
 (2)

where  $\theta_i = i$ th angle, ranging from  $(15i-22.5)^{\circ}$  to  $(15i-7.5)^{\circ}$ ;  $p(\theta_i) =$ percentage of pores with orientation at  $\theta_i$ ;  $N_{\theta i} =$ number of pores with orientation at  $\theta_i$ ; and N =total number of pores.

The pore shape can be characterized by the roundness, defined as follows:

$$R_{\rm s} = \frac{A}{\pi \left(\frac{a}{2}\right)^2} = \frac{b}{a} \tag{3}$$

where  $R_s$  = pore roundness, which varies from approaching 0 for a very elongated pore to near 1 for an equiaxed pore; a = major axis length of the fitting ellipse; b = minor axis length of the fitting ellipse; and A = pore area.

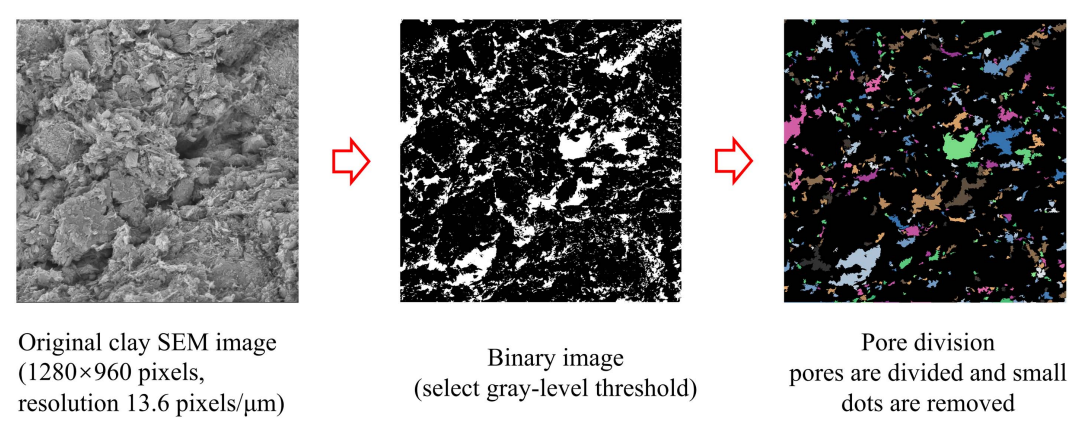


Fig. 15. SEM image processing and pore identification.

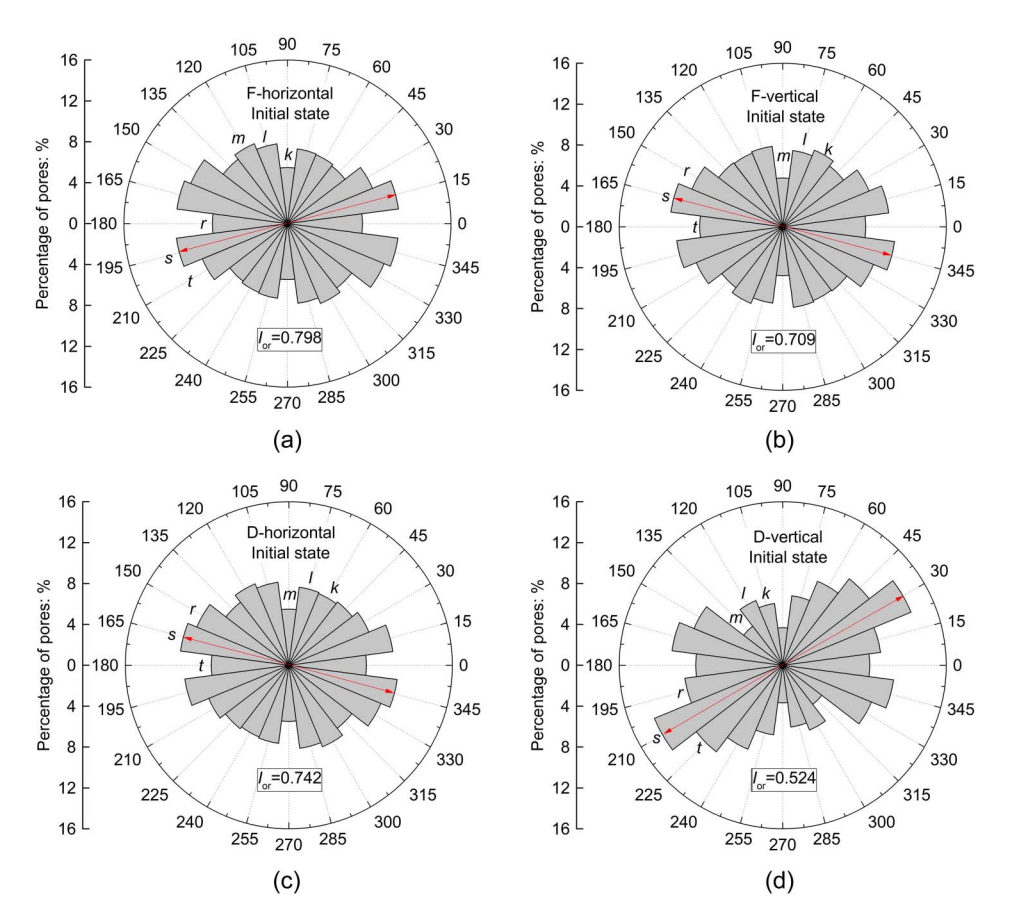


Fig. 16. Rose diagram of pore orientation in (a) horizontal plane; and (b) vertical plane of flocculated sample and in (c) horizontal plane; and (d) vertical plane of dispersed sample (initial state).

The rose diagrams of pore orientation at initial state are shown in Fig. 16, showing the pore orientation frequency in different angle ranges. It is noted that the pore orientation of the two samples on the horizontal plane is similar, and the pore orientation on the vertical plane of the two samples is obviously different. The micropores in the flocculated sample are oriented mainly at 15° and 165°, whilst the preferred orientation of the micropores in the dispersed sample is close to 30°. Therefore, the two types of samples can be observed to have significantly different anisotropy.

To quantify the anisotropy of the two microfabrics, the orientation index proposed by Hicher et al. (2000) is used. It is calculated using the micropores orientation results in the rose diagram as follows:

$$I_{\rm or} = \frac{k+l+m}{r+s+t} \tag{4}$$

where  $I_{\rm or}$  = orientation index, which varies from 1 for an isotropic pore structure to 0 for a perfectly anisotropic structure; s = maximum orientation percentage; r and t = orientation percentages of two zones beside the maximum percentage zone; and k, l, and m = orientation percentages of the zones perpendicular to zones r, s, and t, respectively.

The average values of  $I_{\rm or}$  in the horizontal planes of the two samples are 0.798 and 0.709, while the average values in the vertical planes are 0.742 and 0.524. It is noted that for the flocculated sample, the values of  $I_{\rm or}$  in the horizontal and vertical planes are very close, indicating an isotropic structure. By comparison, the dispersed sample has a more anisotropic structure since the value of  $I_{\rm or}$  in the vertical plane is much less than that in the horizontal plane.

The pore orientation in the dispersed sample aligns horizontally, being perpendicular to the direction of the major principal stress. As reported by Hattab and Fleureau (2011), the microfabric maintains at the beginning (~5% axial strain) of the triaxial loading; thus the initial more anisotropic microfabric in dispersed samples resulting in more considerable shear strength than flocculated samples (Fig. 5). Interestingly, this finding is consistent with the laboratory observation on sand (Vaid et al. 1999; Yang et al. 2008); that is,

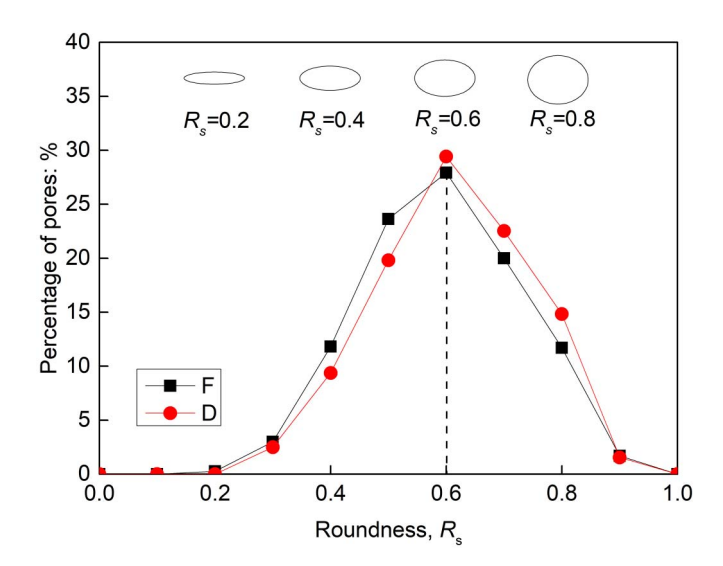


Fig. 17. Pore roundness curves of flocculated and dispersed samples.

a specimen with a higher degree of anisotropy shows larger shear strength than the specimen with a more or less isotropic fabric under otherwise identical conditions.

Fig. 17 shows the pore roundness distribution of the flocculated and dispersed samples at the initial state. The majority of pores within the two samples have roundness between 0.4 and 0.8, with a dominant value of about 0.6, showing clear elliptical shapes. Compared with the flocculated sample, the dispersed sample has a larger number of pores with roundness greater than 0.6, implying that more pores are close to the rounded shape. More rounded pores are likely associated with more dilative behavior (Gao et al. 2020). This may be another cause for smaller pore pressures being generated in dispersed samples than in flocculated samples during undrained loading. It is worth noting that besides initial pore orientation and pore shape, the evolution of the microfabric may also affect the macroscale behavior.

#### Evolution of Microfabric and Its Effect

Besides the initial microfabric, quantitative analysis of microfabric was also conducted for the state after isotropic consolidation (i.e., 200 kPa) and the state at the strain level of 15% due to undrained triaxial compression. The rose diagrams of pore orientation at the two states are shown in Figs. 18 and 19, respectively. The variation of  $I_{\rm or}$  at the three states is shown in Fig. 20 for both flocculated and dispersed samples.

The results in Figs. 18 and 20 suggest that there is a decrease of  $I_{\rm or}$  in the horizontal plane and an increase of  $I_{\rm or}$  in the vertical plane due to isotropic consolidation, implying that an increase of anisotropy occurs in the horizontal plane and a decrease in anisotropy occurs in the vertical plane, for both flocculated and dispersed samples. As the vertical plane is dominant in the triaxial setting, the reorientation of particles during consolidation overall leads to a more isotropic microfabric; this finding is generally consistent with the previous observation (Hicher et al. 2000; Hattab and Fleureau 2011). On the other hand, compared with the flocculated sample, a more anisotropic microfabric in the vertical plane can be found for the dispersed sample after consolidation. When large strain develops (~15%, around the critical state), the rotation of the micropores becomes more apparent, and their orientation progressively tends toward ~165° and ~30° for the flocculated and dispersed samples, respectively.

Furthermore, the preferred orientation of micropores can be observed in the dispersed sample, accompanied by microslip planes [Fig. 21(b)], which implies that the sample can develop strain localization with further loading. Interestingly, the formation of microslip planes cannot be found in the flocculated samples [Fig. 21(a)]. Hattab and Fleureau (2010) observed that slip occurs when the principal orientation develops toward the planes of 20°–40°. In this study, the preferred orientation of pores is about 30° [Fig. 19(d)], indicating similar slip mechanisms. The formation of microslip plane at large deformation may explain why the dispersed

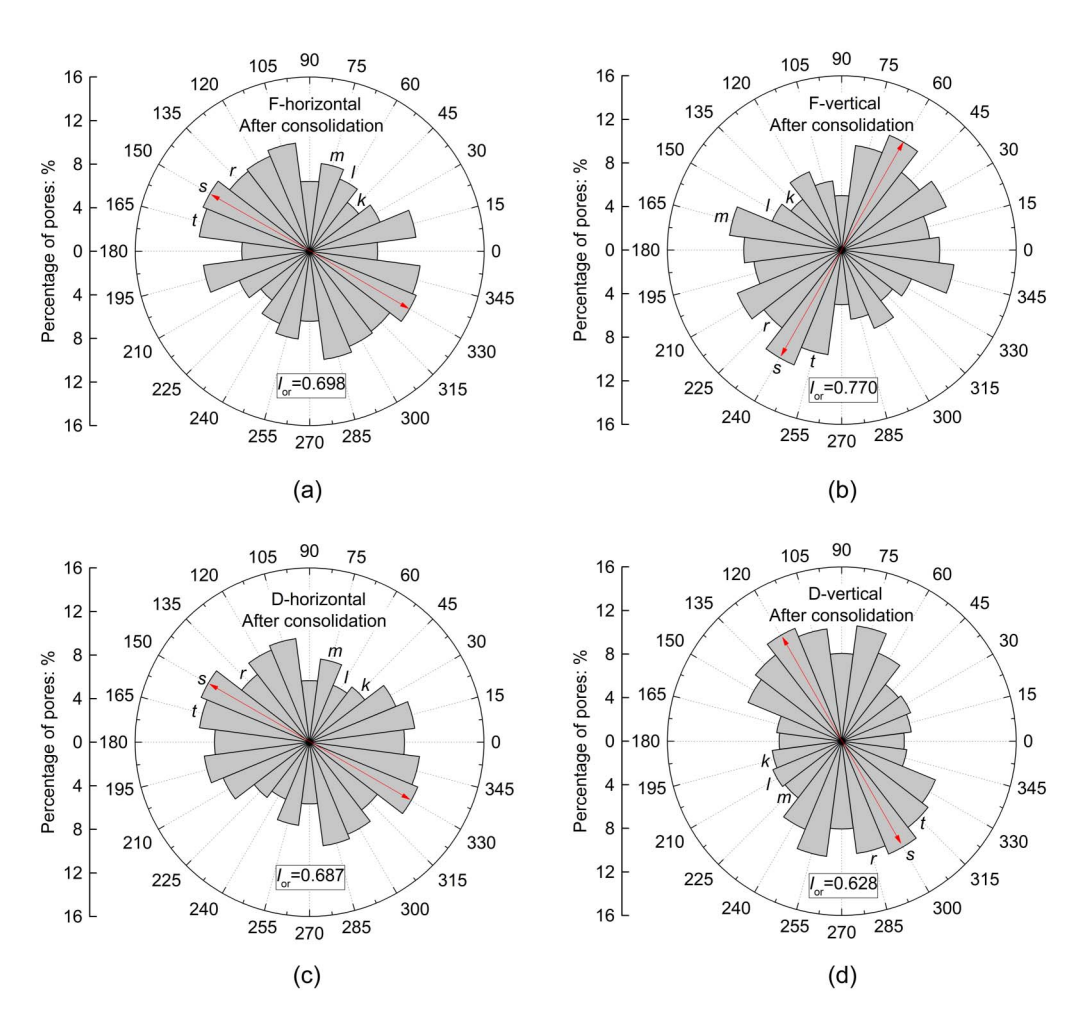


**Fig. 18.** Rose diagram of pore orientation in (a) horizontal plane; and (b) vertical plane of flocculated sample and in (c) horizontal plane; and (d) vertical plane of dispersed sample (after consolidation).

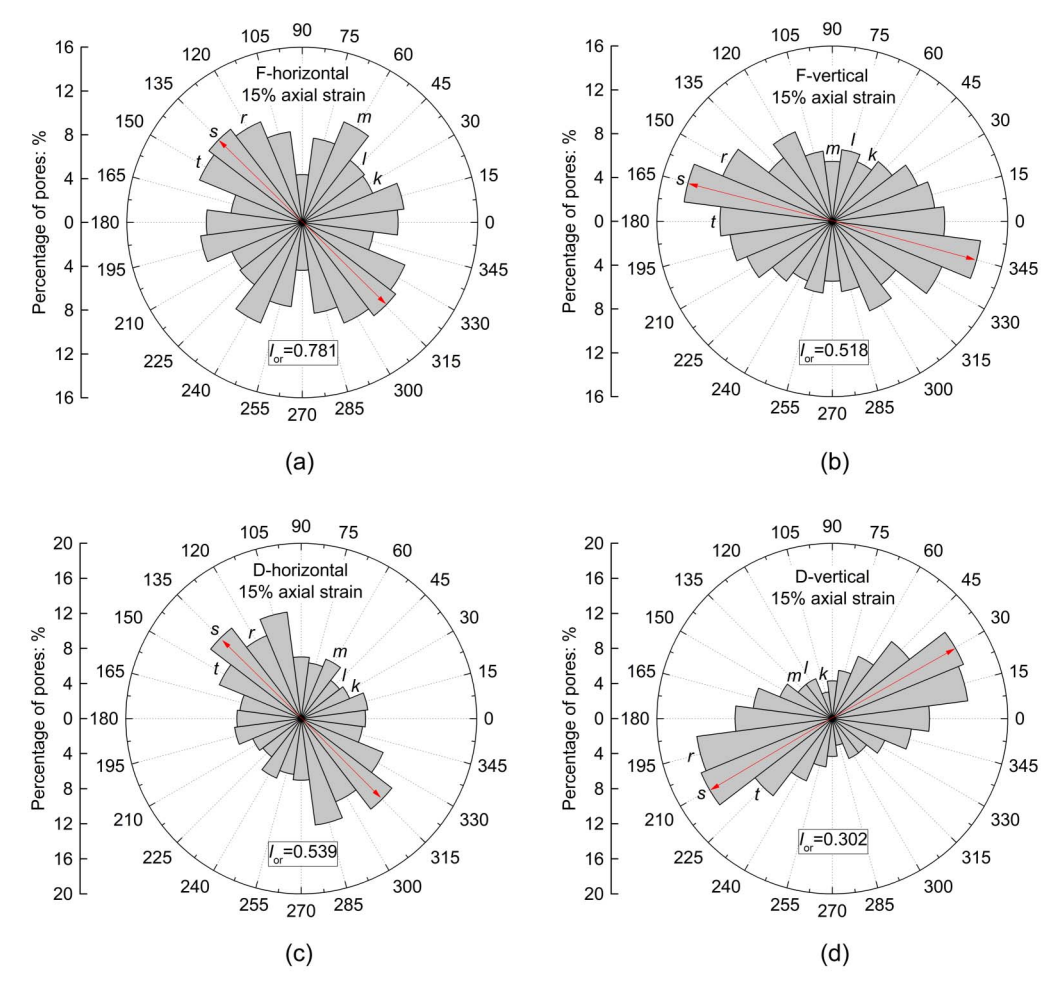


**Fig. 19.** Rose diagram of pore orientation in (a) horizontal plane; and (b) vertical plane of flocculated sample and in (c) horizontal plane; and (d) vertical plane of dispersed sample (15% axial strain).

samples exhibit a kind of strain-softening behavior in the monotonic tests and a rapid plastic strain development in the cyclic tests (Type II' and Type III'). Also, it may help explain why the dispersed samples attain a lower stress ratio at the critical state.

## **Conclusions**

This paper presents new experimental data for better understanding the effect of microfabric on the cyclic behavior of clay. An efficient method was put forward to prepare high quality samples with floculated and dispersed microfabrics. A series of undrained cyclic tests with various CSR was carried out, and a quantitative analysis of the microfabric was conducted. The main results and findings are summarized as follows:

- Microfabric plays a vital role in the undrained cyclic behavior of kaolin clay, including both the accumulation of plastic strains and the buildup of residue pore pressures.
- A critical CSR can be identified for both flocculated and dispersed samples. Depending on the applied CSR with reference to the critical CSR, a clay sample can exhibit markedly different patterns of plastic strain accumulation.
- The microfabric affects the critical CSR, and this effect is coupled with the effective confining pressure. In general, the flocculated sample has a larger critical CSR than the dispersed one.

- For flocculated samples, when the applied CSR is larger than the
  critical CSR, plastic strain accumulates quickly to a large level
  in the initial stage of loading, and it then accumulates at a
  decreased rate. In dispersed samples, however, a rapid development of plastic strain toward failure may occur within first few
  cycles.
- The quantitative analysis of SEM images indicates that the dispersed sample has a more anisotropic microfabric in that particles

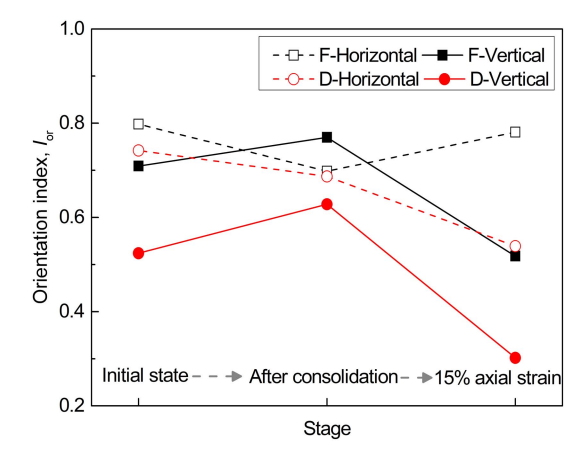
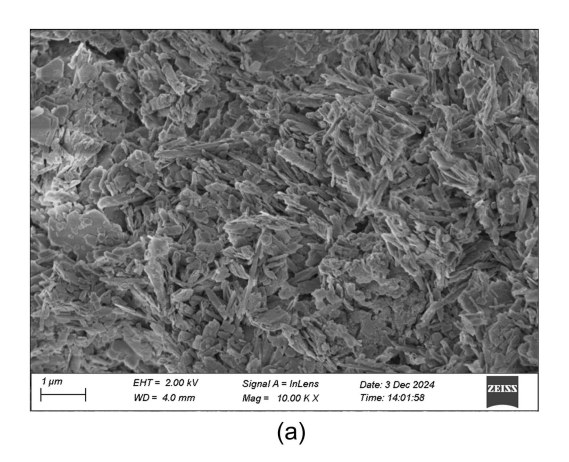


Fig. 20. Microfabric evolution of flocculated and dispersed samples.



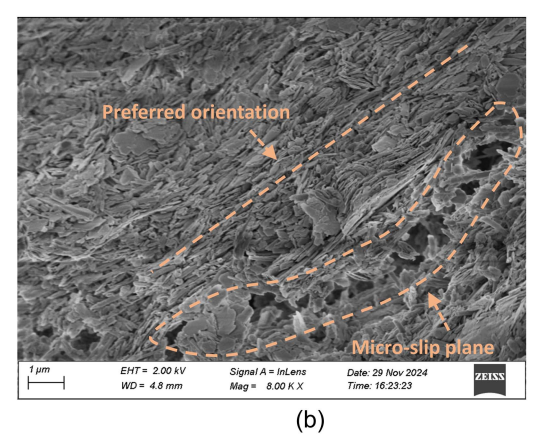


Fig. 21. SEM images at axial strain of 15% for (a) flocculated; and (b) dispersed samples in vertical plane.

- or particle aggregates prefer to orientate horizontally. This may explain why the dispersed sample, when subjected to triaxial compression, exhibits larger strength than the flocculated sample.
- The microfabric of dispersed samples tends to be more anisotropic during undrained shear, and the formation of microslip planes may occur at large stains. This is a plausible microscale mechanism for the macroscopic observation that dispersed samples exhibit a kind of strain-softening behavior in the monotonic tests and a more rapid plastic strain development in the cyclic tests.

# **Data Availability Statement**

Data are available from the corresponding author upon reasonable request.

# **Acknowledgments**

The financial support provided by the National Natural Science Foundation of China (Nos. 52278366 and 51608394) and by the Research Grants Council of Hong Kong (N-HKU723/23) is gratefully acknowledged.

## References

- Broms, B. B., and A. O. Casbarian. 1965. "Effects of rotation of the principal stress axes and of the intermediate principal stress on the shear strength." In Vol. 1 of *Proc.*, 6th Int. Conf. on Soil Mechanics Found. Engineering, 179–183. Oxford, UK: Pergamon Press.
- Carty, W. M. 1999. "The colloidal nature of kaolinite." Am. Ceram. Soc. Bull. 78 (8): 72–76.
- Chow, J. K., Z. Li, and Y.-H. Wang. 2019. "Comprehensive microstructural characterizations of 1-D consolidated kaolinite samples with fabric tensors and pore elongation factors." *Eng. Geol.* 248 (Jan): 22–33. https://doi.org/10.1016/j.enggeo.2018.10.016.
- Delage, P., and G. Lefebvre. 1984. "Study of the structure of a sensitive Champlain clay and of its evolution during consolidation." *Can. Geotech. J.* 21 (1): 21–35. https://doi.org/10.1139/t84-003.
- Delage, P., and F. M. Pellerin. 1984. "Influence de la lyophilisation sur la structure d'une argile sensible du Québec." *Clay Miner*. 19 (2): 151–160. https://doi.org/10.1180/claymin.1984.019.2.03.
- Du, B. L., G. K. Mikroudis, and H.-Y. Fang. 1986. "Effect of pore fluid pH on the dynamic shear modulus of clay." In *Hazardous and indus*-

- trial solid waste testing and disposal: Sixth volume, 226–239. West Conshohocken, PA: ASTM.
- Edil, T. B., and G. F. Luh. 1980. "Microstructural effects on dynamic response of clays." In Vol. 3 of *Proc.*, 7th World Conf. on Earthquake Engineering, edited by O. Ergünay and M. Erdik, 133–140. Ankara, Turkey: Turkish National Committee on Earthquake Engineering.
- Gao, Q.-F., M. Jrad, M. Hattab, J.-M. Fleureau, and L. I. Ameur. 2020. "Pore morphology, porosity, and pore size distribution in kaolinitic remolded clays under triaxial loading." *Int. J. Geomech.* 20 (6): 04020057. https://doi.org/10.1061/(ASCE)GM.1943-5622.0001682.
- Guo, L., J. Wang, Y. Cai, H. Liu, Y. Gao, and H. Sun. 2013. "Undrained deformation behavior of saturated soft clay under long-term cyclic loading." *Soil Dyn. Earthquake Eng.* 50 (Jul): 28–37. https://doi.org/10 .1016/j.soildyn.2013.01.029.
- Hattab, M., and J. M. Fleureau. 2010. "Experimental study of kaolin particle orientation mechanism." *Géotechnique* 60 (5): 323–331. https://doi.org/10.1680/geot.2010.60.5.323.
- Hattab, M., and J. M. Fleureau. 2011. "Experimental analysis of kaolinite particle orientation during triaxial path." *Int. J. Numer. Anal. Methods Geomech.* 35 (8): 947–968. https://doi.org/10.1002/nag.936.
- Hazen, I., and D. Penumadu. 1999. Resonant column testing of clay specimens with controlled microfabric. Rep. No. 99–02. Potsdam, NY: Clarkson Univ.
- Hicher, P. Y., H. Wahyudi, and D. Tessier. 2000. "Microstructural analysis of inherent and induced anisotropy in clay." *Mech. Cohesive-frict. Mater.* 5 (5): 341–371. https://doi.org/10.1002/1099-1484(200007)5:5 <341::AID-CFM99>3.0.CO;2-C.
- Hyde, A., K. Yasuhara, and K. Hirao. 1993. "Stability criteria for marine clay under one-way cyclic loading." *J. Geotech. Eng.* 119 (11): 1771– 1789. https://doi.org/10.1061/(ASCE)0733-9410(1993)119:11(1771).
- Idriss, I. M., Y. Moriwaki, S. G. Wright, E. H. Doyle, and R. S. Ladd. 1980. "Behavior of normally consolidated clay under simulated earthquake and ocean wave loading conditions." In Vol. 1 of *Proc.*, *Int. Sym. Soils under Cyclic Transient Loading*, 437–445. Swansea, Wales: A.A. Balkema.
- Kirkgard, M. M., and P. V. Lade. 1993. "Anisotropic three-dimensional behavior of a normally consolidated clay." Can. Geotech. J. 30 (5): 848–858. https://doi.org/10.1139/t93-075.
- Krizek, R. J., T. B. Edil, and I. K. Ozaydin. 1975. "Preparation and identification of clay samples with controlled fabric." *Eng. Geol.* 9 (1): 13–38. https://doi.org/10.1016/0013-7952(75)90025-3.
- Lambe, T. W., and R. V. Whitman. 1969. Soil mechanics. New York: Wiley.
  Larew, H. G., and G. A. Leonards. 1962. "A strength criterion for repeated loads." In Vol. 41 of Proc., 41st Annual Meeting of the Highway Research Board, 526–556. Washington, DC: Transportation Research Board
- Liu, C., B. Shi, J. Zhou, and C. Tang. 2011. "Quantification and characterization of microporosity by image processing, geometric measurement and statistical methods: Application on SEM images of clay materials."

- Appl. Clay Sci. 54 (1): 97–106. https://doi.org/10.1016/j.clay.2011 .07.022.
- Martin, R. T. 1965. Quantitative fabric of consolidated kaolinite. Reearch Rep. No. R65-47, Soils Publication No. 179. Cambridge, MA: Massachusetts Institute of Technology.
- Mckyes, E. 1971. "Three techniques for fabric viewing as applied to shear distortion of a clay." Clays Clay Miner. 19 (5): 289–293. https://doi.org /10.1346/CCMN.1971.0190504.
- Mitchell, J. 1993. Fundamentals of soil behavior. New York: Wiley.
- Pillai, R. J., R. G. Robinson, and A. Boominathan. 2011. "Effect of microfabric on undrained static and cyclic behavior of kaolin clay." J. Geotech. Geoenviron. Eng. 137 (4): 421–429. https://doi.org/10 .1061/(ASCE)GT.1943-5606.0000442.
- Prakongkep, N., A. Suddhiprakarn, I. Kheoruenromne, and R. J. Gilkes. 2010. "SEM image analysis for characterization of sand grains in Thai paddy soils." *Geoderma* 156 (1–2): 20–31. https://doi.org/10.1016/j .geoderma.2010.01.003.
- Prashant, A., and D. Penumadu. 2005. "A laboratory study of normally consolidated kaolin clay." Can. Geotech. J. 42 (1): 27–37. https://doi. org/10.1139/T04-076.
- Sachan, A., and D. Penumadu. 2007. "Effect of microfabric on shear behavior of kaolin clay." J. Geotech. Geoenviron. Eng. 133 (3): 306–318. https://doi.org/10.1061/(ASCE)1090-0241(2007)133:3(306).
- Sangrey, D. A., G. Castro, S. J. Poulos, and J. W. France. 1978. "Cyclic loading of sands, silts and clays." In *Proc.*, the Specialty Conf. Earthquake Eng. Soil Dynamics, 836–851. Reston, VA: ASCE.
- Seed, H. B., and C. K. Chan. 1959. "Structure and strength characteristics of compacted clays." J. Soil Mech. Found. Div. 85 (5): 87–128. https:// doi.org/10.1061/JSFEAQ.0000229.
- Seed, H. B., and C. K. Chan. 1966. "Clay strength under earthquake loading conditions." J. Soil Mech. Found. Div. 92 (2): 53–78. https://doi.org/10.1061/JSFEAQ.0000867.
- Sides, G., and L. Barden. 1971. "The microstructure of dispersed and flocculated samples of kaolinite, illite, and montmorillonite." Can. Geotech. J. 8 (3): 391–399. https://doi.org/10.1139/t71-041.
- Sloane, R. L. 1966. "The fabric of mechanically compacted kaolin." Clays Clay Miner. 14 (1): 289–292. https://doi.org/10.1016/B978-0-08 -011908-3.50027-X.

- Soga, K. 1994. "Mechanical behavior and constitutive modelling of natural structured soils." Ph.D. thesis, Dept. of Civil Engineering, Univ. of California at Berkeley.
- Sokolov, V. N., D. I. Yurkovets, O. V. Ragulina, and V. N. Melnik. 1998. "Computer-controlled system for the study of micromorphology of the surface of solids by SEM images." Surface Invest. 14 (5): 33–41.
- Sze, H. Y., and J. Yang. 2014. "Failure modes of sand in undrained cyclic loading: Impact of sample preparation." J. Geotech. Geoenviron. Eng. 140 (1): 152–169. https://doi.org/10.1061/(ASCE)GT.1943-5606 .0000971.
- Tang, C.-S., L. Lin, Q. Cheng, C. Zhu, D.-W. Wang, Z.-Y. Lin, and B. Shi. 2020. "Quantification and characterizing of soil microstructure features by image processing technique." *Comput. Geotech.* 128 (Dec): 103817. https://doi.org/10.1016/j.compgeo.2020.103817.
- Vaid, Y. P., S. Sivathayalan, and D. Stedman. 1999. "Influence of specimen reconstituting method on the undrained response of sand." ASTM Geotech. Test. J. 22 (3): 187–195. https://doi.org/10.1520/GTJ11110J.
- Wang, Y. H., and W. K. Siu. 2006. "Structure characteristics and mechanical properties of kaolinite soils. II. Effects of structure on mechanical properties." Can. Geotech. J. 43 (6): 601–617. https://doi.org/10.1139/t06-027.
- Wheeler, S. J., and V. Sivakumar. 2000. "Influence of compaction procedure on the mechanical behavior of an unsaturated compacted clay. Part 2: shearing and constitutive modeling." *Géotechnique* 50 (4): 369–376. https://doi.org/10.1680/geot.2000.50.4.369.
- Wood, D. M. 1990. Soil behaviour and critical state soil mechanics. Cambridge, UK: Cambridge University Press.
- Yang, J., and H. Y. Sze. 2011. "Cyclic strength of sand under sustained shear stress." J. Geotech. Geoenviron. Eng. 137 (12): 1275–1285. https://doi.org/10.1061/(ASCE)GT.1943-5606.0000541.
- Yang, Z. X., X. S. Li, and J. Yang. 2008. "Quantifying and modelling fabric anisotropy of granular soils." *Géotechnique* 58 (4): 237–248. https://doi.org/10.1680/geot.2008.58.4.237.
- Yasuhara, K., and K. H. Andersen. 1991. "Recompression of normally consolidated clay after cyclic loading." Soils Found. 31 (1): 83–94. https://doi.org/10.3208/sandf1972.31.83.
- Yu, C. Y., J. K. Chow, and Y.-H. Wang. 2016. "Pore-size changes and responses of kaolinite with different structures subject to consolidation and shearing." Eng. Geol. 202 (Mar): 122–131. https://doi.org/10.1016/j.enggeo.2016.01.007.